Electronic Coupling in π-Conjugated Molecule Bridged Silicon Quantum Dot Clusters Synthesized by Sonogashira Cross–Coupling Reaction

Thu-Huong Le[†], Young-Hwa Choi[†], Ki-Jeong Kim[‡], and Hyun-Dam Jeong[*,†]

[†]*Department of Chemistry, Chonnam National University, Gwangju, 61186, Republic of Korea*
[‡]*Pohang Accelerator Laboratory, Pohang University of Science and Technology, Pohang 790-784, Republic of Korea*

Experimental (in the Supporting Information)

Toluene (anhydrous, 99.8 %), tetraethylorthosilicate ($Si(OC_2H_5)_4$, ≥ 99 %), Brij® L4 surfactant ($(C_{20}H_{42}O_5)_n$), and 1-hexanol ($CH_3(CH_2)_5OH$, 98 %) were purchased from Sigma-Andrich. Cyclohexane (C_6H_{12}, 99.8 %), n-hexane (C_6H_{14}, 95 %), ethanol (C_2H_5OH, 99.5 %), acetone, and chloroform ($CHCl_3$, 99.7 %) were purchased from Dae-Jung (South Korea), ammonium hydroxide solution (NH_4OH, 25 %) was purchased from Acros Organic, and magnesium powder (Mg, -100+200 mesh, 99.6 %) was purchased from Alfa Aesar, respectively.

• **Synthesis of silica nanoparticle.** The SiO_2 NPs were synthesized from tetraethylorthosilicate (TEOS) molecules by a micro-emulsion method using reverse micelles, as shown in Scheme S1 a. Brij® L4 surfactant (24 g) was mixed with cyclohexane (400 mL) and 1-hexanol (6.4 mL) by sonication for 90 min, until the mixture changed to a clear solution. Distilled water (8 mL) was then added, and the reaction mixture was sonicated for 30 min. When the water was added, a white solid was generated in the reaction mixture, which was completely re-dissolved by sonication. TEOS (10 mL) was then added with stirring, and the reaction mixture was further stirred for 90 min at room temperature. For the hydrolysis and condensation of TEOS, NH_4OH (1.6 mL) was slowly added while stirring the reaction mixture, which was then stirred for an

addition 12 h at room temperature. After the reaction had been completed, the reverse micro-emulsion was destabilized by adding acetone (400 mL), followed by centrifugation at 12,000 rpm for 5 min. The SiO_2 NPs powder was washed with acetone (30 ml for each wash) (4–5) times, ethyl alcohol (30 ml for each wash) (4–5) times, and water (30 ml for each wash) (4–5) times.

• **Synthesis of silicon nanocrystal.** Previously, Veinot et al. demonstrated the synthesis of silicon nanocrystal using magnesiothermic reduction methods.[1] Magnesiothermic reduction offers a straightforward way to convert silica (inexpensive and the most stable source of Si) into elemental silicon, while retaining the silica particle morphology. Nevertheless, the massive heat release from the exothermic reaction ($Mg + SiO_2 \rightarrow Si + MgO$, $\Delta H = -586.7$ kJ/mol$_{silica}$)[2] collapsed the structure of SiO_2 NP, and agglomerated silicon crystal into the larger crystal. In our report, the SiO_2 NPs powder (1 g, 0.016 mol w.r.t Si content), sodium chloride (NaCl, 10 g), and magnesium powder (0.9 g, 0.0375 mol) were mixed (Scheme S1 a), ball-milled, and ground together manually to give a grayish brown-colored powder, then heated at 670 °C for 15 h under an argon atmosphere in a quartz tube furnace. The use of NaCl as a heat scavenger during the reduction process ($Mg + SiO_2 \rightarrow Si + MgO$) prevents the structure collapsing, and aggregating into the larger crystal of silicon domain. The resulting dark brown colored powder product was washed to remove NaCl, and treated with hydrochloric acid (20 mL) for 12 h to remove the Mg remaining, Mg_2Si, and MgO. A brown precipitate was obtained by vacuum filtration. Then the solid was washed with distilled water, until the washings resulted in a neutral pH (ca. 7). The precipitate was then washed with ethanol (30 mL) and acetone (3 × 30 mL), and air-dried to yield oxide-coated Si NCs (Si NCs@SiO_2). Finally, the Si NC@SiO_2 was obtained as a brown powder.

• **Synthesis of 4-ethynylstyryl and octyl co-capping Si QD.** The hydride-terminated silicon quantum dots (H–Si QDs) were synthesized from only the Si NCs@SiO_2 (0.5 g) through an

etching reaction using 1:1:1 mixture of hydrofluoric acid, ethanol, and distilled water for 6 hours (Scheme S1 b). After completing the etching process, H–Si QDs were extracted from the etching solution with dry toluene. Then, H–Si QDs were isolated from the toluene by centrifugation at 12,000 rpm for 5 min. To stabilize the Si QDs surface and obtain the required chemical functionality and solubility in a solvent, the surface of the Si QDs was passivated through the attachment of organic molecular ligands. In this article, the colloidal Si QD surface was modified by 1,4-diethynylbenzene and 1-octene capping, in which 1-octene was used as co-capping. The H–Si QDs were dispersed in anhydrous toluene, and then capped with 1,4-diethynylbenzene and 1-octene by hydrosilylation under BH_3·THF catalysis at room temperature to give 4-ethynylstyryl and octyl co-capping Si QD (4-Es/Oct Si QD) (Scheme S1 b).[3] As we recently reported, the 4-ethynylstyryl and octyl co-capping allow the Si QD surface to be more protected from the oxidation and more soluble in solvent, compared with only 4-ethynylstyryl capping.[4] This is thought to be the structural rigidity of 4-ethynylstyryl capping groups inducing incomplete surface passivation of Si QD, as compared to the flexible octyl capping due to the strong conjugation between the Si QD and the 4-ethynylstyryl capping molecule. Moreover, most of the π–conjugated poly(aryleneethynylene)'s so far reported have only low solubility, and were not suited to the investigation of their optical properties.[5] On the other hand, it has been reported that the use of alkyl-substituent arylene in π–conjugated poly(aryleneethynylene) enhances the solubility of the polymer in organic solvent. Therefore in this article, the H–Si QD surface was modified by 1,4-diethynylbenzene and 1-octene capping, in which 1-octene is used as co-capping. For surface functionalization of silicon nanocrystal, Purkait et al. have reported that the borane-tetrahydrofuran complex solution was used as catalysts for functionalization of the hydride-terminated silicon nanocrystal with alkenes/alkynes.[3] Thus, the H–Si QD surface was passivated by hydrosilylation with 1,4-diethynylbenzene and 1-octene under BH_3·THF catalysis at room temperature. BH_3·THF solution (0.6 mL, 1 M solution in THF) was added slowly to the reaction mixture with stirring at 0 °C under Ar condition (Scheme S1 b). The reaction mixture was allowed to warm to room

temperature. The reaction mixture was degassed by three cycles of evacuation, purging with argon to eliminate water, and stirring for 48 h. Following functionalization, the reaction mixture was transferred into test tubes, and centrifuged at 12,000 rpm to remove any aggregated or unreacted material. The supernatant was filtered through a 0.25 μm PTFE filter. The reaction mixture in toluene was extracted with water (3 times) to remove BH_3·THF catalysis, and brine (2 times), and dried over anhydrous $MgSO_4$. The product was collected by toluene, and the toluene solvent was removed at about 40 °C under reduced pressure to obtain dried solid. The remaining 1,4-diethynylbenzene capping molecules were separated by the column chromatography of silica-gel ((40–63) μm) using solvent *n*-hexane. The 4-Es/Oct Si QD was separated by using a solvent system of *n*-hexane-chlorofrom 3:1. However, due to interaction between 4-Es/Oct Si QD and 1,4-diethynylbenzen through C≡C–H···C≡C hydrogen bonds,[5] the removal processed by remaining capping molecules 1,4-diethynylbenzene was not completed. Finally, the product was obtained as yellow powder to include 4-Es/Oct Si QD and the remaining capping molecules of 1,4-diethynylbenzene.

- **Synthesis of π–conjugated Poly(aryleneethynylene) (PAE).** Polymerization was synthesized by Sonogashira C–C coupling reaction (Scheme S1 c). C–C coupling reaction between 1,4-diethynylbenzene and 2,5-dibromo-3-hexyl-thiophene was carried out in the argon atmosphere by using standard Schleck techniques. The 1,4-diethynylbenzene (0.1 g), $Pd(PPh_3)_2Cl_2$ (20 mg), and CuI (8 mg) were dispersed in a mixture of anhydrous toluene (6 mL) and triethylamine (TEA, 3 mL), and then added to a 100 ml two-neck flask equipped with a condenser that was connected to a Schleck line filled with argon via a cannula.[6, 7] The solution was stirred for 5 min at room temperature. The 2,5-dibromo-3-hexyl-thiophene (0.2 g) and anhydrous toluene (6 mL) were added to the mixture, and the reaction mixture was stirred at 110 °C for 2.5 h to obtain a brown solution. After cooling the reaction mixture, methanol (MeOH) was added to the reaction mixture, and then centrifuged at 15,000 rpm for 5 min to

obtain a brown powder. This powder was washed with MeOH repeatedly (3 times) to remove the catalyst.

Results and Discussion (in the Supporting Information)

• **X-ray diffraction result of 4-ethynylstyryl and octyl co-capping Si QD.** The Si QDs size and crystal structure were also confirmed from XRD (Fig. S1). The peak of the (111) plane at 28.3° in the XRD patterns indicates that Si QDs had a diamond structure,[1] and the mean size Si QDs diameter was estimated using the Scherrer equation to be 4.5 nm. Due to hydrogen boding interaction between parallel aligned ethynyl groups between 4-Es/Oct Si QD and 1,4-diethynylbenzene through C≡C–H···C≡C, the removal of the remaining capping molecule, 1,4-diethynylbenzene, is not completed. Eichhorn et al. reported that the bulk structure of 1,4-diethynylbenzene is stabilized by C≡C–H···C≡C hydrogen bonding.[5] The XRD result of 4-Es/Oct Si QD (Fig. S1 of the SI) shows the peak (★) at 24.9°, which is related to the remaining molecular capping (1,4-diethethynylbenzene). Thus, the 4-Es/Oct Si QDs were obtained as yellow solid including remaining 1,4-diethynylbenzene molecules, as seen in Scheme S1 b.

• **H-NMR and UV-vis absorption spectra of P.1 and P.2.** The chemical structure analyses of **P.1** and **P.2** were characterized by H-NMR (Figs. S2 a and b) in comparison with those of poly(aryleneethynylene), 2,5-dibromo-3-hexylthiophene, and 4-Es/Oct Si QD. As for the H-NMR spectrum of **P.2**, we can see first the appearance of signals from capping groups on Si QD, which are found at 6.9 ppm (Si–CH=C), 6.7 ppm (CH=C–), and 3.1 ppm (≡C−H) from 4-ethynylstyryl capping,[8] and 1.2 ppm ($–CH_2–$), 0.8 ppm ($–CH_3$) from octyl capping. Here, we also see 2.4 ppm ($C=C–CH_2–$), 1.5 ppm ($CH_2–$), and 0.8 ppm ($–CH_3$) from hexyl group of thiophene.[9, 10] On the other hand, the H-NMR spectrum of **P.1** show only signals of protons of hexyl group of thiophene, which are mostly at 1.5 ppm ($CH_2–$) and 0.8 ppm ($–CH_3$),[10] strongly implying little involvement of Si QD. In addition, Fig. S3 shows the UV-vis absorption spectra of **P.2** (red line) and **P.1** (green line), in comparison with 4-Es/Oct Si QD (black solid line) and

poly(aryleneethynylene) (black dot line) in chloroform. First, **P.2** (red line) and 4-Es/Oct Si QD (black solid line) have the absorption at 260 nm (4.7 eV), which indicates the presence of silicon quantum dot in **P.2. P.1** (green line) do show relatively weak absorption at 260 nm (4.7 eV), implying little involvement of silicon quantum dot in **P.1**, while poly(aryleneethynylene) (black dot line) do not show any absorption at 260 nm. Second, **P.2** (red line) and **P.1** (green line) have absorption at 340 nm (3.6 eV), which is attributed to attributed to the change of electronic structure of Si QD upon clustering. Concretely, it is surely generated from the extension of conjugation length with thiophene ring and adjacent Si QDs. Though, the absorption intensity for **P.1** is smaller than that for **P.2,** implying little involvement of silicon quantum dot in **P.1.** Therefore, combining the UV-vis absorption results with the H-NMR data, we conclude that **P.2** is the main product containing Si QDs, and **P.1** is a byproduct of of high fraction of very long π–conjugated polymer chain. We name the main product of Si QD (**P.2**) as "Si QD cluster", by considering the morphology of the cluster, confirmed by the TEM results (Fig. 1 b and d).

• **FT-IR spectra of Si QDs cluster (A; P2).** Figure S4 shows the FT–IR spectra of Si QDs cluster (**A**; **P2**) compared to 4-Es/Oct Si QD. The peaks at 2951, 2924, and 2854 cm^{-1} indicate the presence of octyl groups in the Si QDs.[11] Whereas, the peaks at 3034 and 1601 cm^{-1} were assigned to the sp^2-hybridized C–H stretching and C=C bond in conjugation with Si atoms on QD surface (Si–C=C-),[9, 12, 13] respectively. After cross-coupling reaction, the peak intensity at 3292 cm^{-1} corresponding to ≡C–H stretching band of π–conjugated Si QDs cluster gradually decreases as compared with that of 4-Es/Oct Si QD. In addition, the υ (C≡C) stretching band of Si QD cluster appears at 2164 cm^{-1}, while the υ (C≡C) stretching band of 4-Es/Oct Si QD is at 2107 cm^{-1}. Yamamoto et al. have reported that the polycondensation for poly (arylene ethynylene) shifts the υ (C≡C) band of the original HC≡C–Ar–C≡CH to higher frequency, which is consistent with a known trend that di-substituted acetylenes RC≡CR' give rise to the υ (C=C) band at a frequency higher than that for mono-substituted acetylenes RC≡CH.[6] Then,

these FT-IR results indicate that that 4-Es/Oct Si QD and 2,5-dibromo-3-hexylthiophene are C–C cross-coupled together in the Si QD cluster.

• **The relationship between conductance (G) and diffusion coefficient (*D*).** At low bias, the current–voltage (I–V) characteristics show ohmic behavior,[14] so that the conductance (*G*) was obtained by the following equation:

$$G = \frac{I}{V} \quad \text{(A1)}$$

The conductance of a given thin film depends on its cross-sectional area (*A*) and length (*l*). Then, the conductance G can be expressed as

$$G = \sigma\frac{A}{l} \quad \text{(A2)}$$

where, σ is the electrical conductivity measured in siemens per meter ($S{\cdot}m^{-1}$). The conductivity σ is determined by carrier concentration (*n*), elementary charge (*e*), and carrier mobility (μ):

$$\sigma = ne\mu \quad \text{(A3)}$$

The carrier mobility (μ) is defined as the ratio of carrier drift velocity (v_d) to the applied electric field (*E*):

$$\mu = \frac{v_d}{E} \quad \text{(A4)}$$

In our studies, we tentatively assume for simplicity in building up the theoretical formalism that the carriers are electrons, though we have no experimental results about which kind of carriers between electrons and holes are actually working. We consider that this assumption has no effect on the key concepts and discussions in our study, since even the hole carrier follows essentially all the same physics as the electron does. From now on, we are mentioning all physical properties, and even microscopic concepts, only in terms of electron. The macroscopic property of 'electron mobility' μ is now related to another important macroscopic property of the electron diffusion coefficient *D* with the Einstein relation:[15, 16]

$$\mu = \frac{e}{k_B T}D \quad \text{(A5)}$$

As an intermediate summary, we can make the mathematical relationship between *G* and *D*:

$$G = \sigma \frac{A}{l} \quad \text{(A6)}$$

$$G = ne\mu \frac{A}{l} \quad \text{(A7)}$$

$$G = \left(\frac{Ane^2}{lk_BT}\right)D \quad \text{(A8)}$$

- **The relationship between the natural log of G and the reciprocal of absolute temperature.** In the results and discussion in the manuscript, we have obtained the following four equations.

$$D = \frac{1}{2d}\sum_i r_i^2 W_i P_i \quad \text{(B1)}$$

$$P_i = W_i \Big/ \sum_i W_i \quad \text{(B2)}$$

$$D_{mono} = \frac{1}{6}(r^*_{mono})^2 W^*_{mono} \quad \text{(B3)}$$

$$D_{cluster} = \frac{1}{6}(r^*_{cluster})^2 W^*_{cluster} \quad \text{(B4)}$$

After inserting Eqs. (B3) and (B4) into Eq. (A8), we can obtain the conductance G and interdot electron transfer rate *W*.

$$G_{mono} = \left(\frac{An_{mono}e^2}{lk_BT}\right)D_{mono} = \left(\frac{Ae^2}{6lk_BT}\right) n_{mono}\,(r^*_{mono})^2 W^*_{mono} \quad \text{(B5)}$$

$$G_{cluster} = \left(\frac{An_{cluster}e^2}{lk_BT}\right)D_{cluster} = \left(\frac{Ae^2}{6lk_BT}\right) n_{cluster}\,(r^*_{cluster})^2 W^*_{cluster} \quad \text{(B6)}$$

$$ln(G_{mono}) = ln\left(\frac{Ae^2}{6lk_B}\right) + ln(n_{mono}) + 2ln(r^*_{mono}) + ln\left(\frac{1}{T}\right) + ln\left(W^*_{mono}\right) \quad \text{(B7)}$$

$$ln(G_{cluster}) = ln\left(\frac{Ae^2}{6lk_B}\right) + ln(n_{cluster}) + 2ln(r^*_{cluster}) + ln\left(\frac{1}{T}\right) + ln\left(W^*_{cluster}\right) \quad \text{(B8)}$$

Here, we first assume that the electron carrier concentration of 4-Es/Oct Si QD thin film, n_{mono} is quite similar to that of the Si QD cluster thin film, $n_{cluster}$:

$$n_{mono} \cong n_{cluster} \quad \text{(B9)}$$

As for the conventional bulk n-doped Si semiconductor, the electron carrier concentration is usually determined by the n doping concentration. In our Si QD system, although there is no

artificial doping element, the electron carrier concentration might be invoked by the $1S_e$ orbital in Si QD, or defects existing in the Si QD surface. We assume, as mentioned just below, that the interdot distance between QDs in 4-Es/Oct Si QD thin film is the same as that for the Si cluster thin film. Then, the number of $1S_e$ orbital in a unit volume for 4-Es/Oct Si QD thin film is the same as that for the Si cluster thin film. In addition, since the 4-Es/Oct Si QDs and Si QD cluster have locally the same capping groups, we think that their defect concentrations and the relevant electron carrier concentrations over the entire thin films are roughly similar to each other for the two cases. These rough arguments support the above assumption of the same electron carrier concentrations for the 4-Es/Oct Si QD and Si QD cluster thin films. In addition, we secondly assume that the interdot distance r^*_{mono} of 4-Es/Oct Si QD thin film is the same as the effective, representative interdot distance $r^*_{cluster}$ of Si QD cluster thin film:

$$r^*_{mono} \cong r^*_{cluster} \tag{B10}$$

The density of Si QD in Si QD thin films, N_{QD}, is assumed to be roughly proportional to the weight concentration of its precursor solution (C_{QD}) normalized thickness (l) with the proportional constant, if we ignore the relatively small amount of organic linker fragments:

$$N_{QD} \cong k\frac{C_{QD}}{l} \tag{B11}$$

We use the thickness values of 4-Es/Oct Si QD and Si QD cluster thin films, of (70 and 60) nm, respectively, which are measured from their vertical cross-sectional images (Fig. 4). Then, we can compare the density of 4-Es/Oct Si QD thin film with that of Si QD cluster thin film with the same weight concentrations (2 wt.%) of their precursor solutions:

$$\frac{N_{Si\ QD\ cluster}}{N_{4-Es/Oct\ Si\ QD}} \cong \frac{l_{4-Es/Oct\ Si\ QD}}{l_{Si\ QD\ cluster}} = \frac{70\ nm}{60\ nm} = 1.2 \tag{B12}$$

Finally, it is sufficiently plausible to suggest the above assumption of roughly the same interdot distance for the 4-Es/Oct Si QD and Si QD cluster thin films.

$$\frac{r^*_{mono}}{r^*_{cluster}} = \left(\frac{N_{Si\ QD\ cluster}}{N_{4-Es/Oct\ Si\ QD}}\right)^{\frac{1}{3}} = 1.06 \cong 1.0 \tag{B13}$$

The decrease in porosity of Si QD cluster thin films, as compared with that of 4-Es/Oct Si QDs, may result in little decreases in film thickness and interdot center-to-center distance (r^*), which

are ignored as shown in Eq. (B13).

Based on the above two assumptions of the same carrier concentrations and interdot distances, we set the first three terms on the right side of Eqs. (B7) and (B8) as an appropriate constant B:

$$ln\left(\frac{Ae^2}{6lk_B}\right) + ln(n_{mono}) + 2ln(r^*_{mono}) \cong ln\left(\frac{Ae^2}{6lk_B}\right) + ln(n_{cluster}) + 2ln(r^*_{cluster}) \equiv B \quad \text{(B14)}$$

Then, we set two available intermediate equations for the natural log of the conductances of the QD thin films, if tolerating very small errors:

$$ln(G_{mono}) \cong B + ln\left(\frac{1}{T}\right) + ln\left(W^*_{mono}\right) \quad \text{(B15)}$$

$$ln(G_{cluster}) \cong B + ln\left(\frac{1}{T}\right) + ln\left(W^*_{cluster}\right) \quad \text{(B16)}$$

Substituting Eq. (4) for the electron transfer rate *W* into these expressions, we finally obtain the final Eqs. (B17-b) and (B18-b) for the natural log of conductances, where the activation energies, $E_{a,\,mono}$, $E_{a,\,cluster}$ appear in the slope for the linear equation in terms of 1/T:

$$ln(G_{mono}) \cong B + ln\left(\frac{1}{T}\right) + \ln\left[\frac{2\pi}{\hbar}\cdot(V_{mono})^2\left(\frac{1}{16k_B\pi E_{a,mono}}\right)^{\frac{1}{2}}\right] + ln\left[\left(\frac{1}{T}\right)^{\frac{1}{2}}\right] - \frac{E_{a.mono}}{k_B}\left(\frac{1}{T}\right) \quad \text{(B17-a)}$$

$$ln(G_{mono}) - \frac{3}{2}ln\left(\frac{1}{T}\right) \cong B_{mono} - \frac{E_{a,\,mono}}{k_B}\left(\frac{1}{T}\right) \quad \text{(B17-b)}$$

$$B_{mono} = B + \ln\left[\frac{2\pi}{\hbar}\cdot(V_{mono})^2\left(\frac{1}{16k_B\pi E_{a,mono}}\right)^{\frac{1}{2}}\right] \quad \text{(B17-c)}$$

$$ln(G_{cluster}) \cong B + ln\left(\frac{1}{T}\right) + \ln\left[\frac{2\pi}{\hbar}\cdot(V_{cluster})^2\left(\frac{1}{16k_B\pi E_{a,cluster}}\right)^{\frac{1}{2}}\right] + ln\left[\left(\frac{1}{T}\right)^{\frac{1}{2}}\right] - \frac{E_{a.\,cluster}}{k_B}\left(\frac{1}{T}\right) \quad \text{(B18-a)}$$

$$ln(G_{cluster}) - \frac{3}{2}ln\left(\frac{1}{T}\right) \cong B_{cluster} - \frac{E_{a,\,cluster}}{k_B}\left(\frac{1}{T}\right) \quad \text{(B18-b)}$$

$$B_{cluster} = B + \ln\left[\frac{2\pi}{\hbar}\cdot(V_{cluster})^2\left(\frac{1}{16k_B\pi E_{a,cluster}}\right)^{\frac{1}{2}}\right] \quad \text{(B18-c)}$$

References

1. Dasog, M.; Yang, Z.; Veinot, J. G. C. Size-controlled Solid State Synthesis of Luminescent Silicon Nanocrystals Using Stober Silica Particles. *CrysEngComm*, **2012**, *14*, 7576–7578.

2. Luo, W.; Wang, X.; Meyers, C.; Wannenmacher, N.; Sirisaksoontorn, W.; Lerner, M. M.; Ji, X. Efficient Fabrication of Nanoporous Si and Si/Ge Enabled by a Heat Scavenger in Magnesiothermic Reactions. *Sci. Rep.* **2013**, *3*, 2222–2228.

3. Purkait, T. K.; Iqbal, M.; Wahl, M. H.; Gottschling, K.; Gonzalez, C. M.; Islam, M. A.; Veinot, J. G. C. Borane-Catalyzed Room-Temperature Hydrosilylation of Alkenes/Alkynes on Silicon Nanocrystal Surfaces. *J. Am. Chem. Soc.* **2014**, *136*, 17914–17917.

4. Le, T. H.; Kim, K. J.; Jeong, H. D. Effect of Thermal Cross-Linking of 4-Ethynylstyryl Capping Groups on Electronic Coupling between Silicon Quantum Dots in Silicon Quantum Dot Solids. *J. Phys. Chem. C* **2017**, *121*, 15957–15969.

5. Eichhorn, J.; Heckl.; W. M.; Lackinger, M. On-surface Polymerization of 1,4-Diethynylbenzene on Cu(111). *Chem. Commun.* **2013**, *49*, 2900–2902.

6. Yamamoto, T.; Yamada, W.; Takagi, M.; Kizu, K.; Maruyama, T.; Ooba, N.; Tomaru, S.; Kurihara, K.; Kaino, T.; Kubota, K. π-Conjugated Soluble Poly(aryleneethyny1ene) Type Polymers. Preparation by Palladium-Catalyzed Coupling Reaction, Nonlinear Optical Properties, Doping, and Chemical Reactivity. *Macromolecules* **1994**, *27*, 6620–6626.

7. Yamamoto, T.; Takagi, M.; Kizu, K.; Maruyama, T.; Kubota, K.; Kanbara, H.; Kurihara, T.; Kaino, T. Preparation and Optical Properties of Soluble x-Conjugated Poly(aryleneethyny1ene) Type Polymers. *J. Chem. Soc., Chem. Commun.* **1993**, 797–798.

8. Maehara, T.; Ohshita, J.; Taketsugu, R.; Hino, K.; Kunai. A. Hydrosilylation Polymerization for the Synthesis of Organosilicon Polymers Containing Adamantane Units. *Polymer Journal* **2009**, *41*, 973–977.

9. Mukbaniani, O.; Tatrishvili, T.; Titvinidze, G.; Mukbaniani, N.; Lezhava, L.; Gogesashvili, N. Hydrosilylation Reaction of Methylhydridesiloxane to Phenylacetylene. *J. Appl. Polym. Sci.* **2006**, *100*, 2511–2515.

10. Li, J.; Pang, Y. Regiocontrolled Synthesis of Poly[(p-phenylen eethynylene)-*alt*-(2,5-thienylene ethynylene)]s: Regioregularity Effect Photoluminescence and Solution Properties. *Macromolecules* **1998**, 31, 5740–5745.

11. Yang, C. S.; Bley, R. A,; Kauzlarich, S. M.; Lee, H. W. H.; Delgado, G. R. Synthesis of Alkyl-Terminated Silicon Nanoclusters by A Solution Route. *J. Am. Chem. Soc.* **1999**, *121*,

5191–5195.

12 Dung, M. X.; Tung, D. D.; Jeong, S.; Jeong, H. D. Tuning Optical Properties of Si Quantum Dots by π–Conjugated Capping Molecules. *Chem. Asian J.* **2013**, *8*, 653–664.

13. Buriak, J. M.; Stewart, M. P.; Geders, T. W.; Allen, M. J.; Choi, H. C.; Smith, J.; Raftery, D.; Canham, L. T. Lewis Acid Mediated Hydrosilylation on Porous Silicon Surfaces. *J. Am. Chem. Soc.* **1999**, *121*, 11491–11502.

14. Chen, T,; Skinner, B,; Xie, W.; Shklovskii, B. I.; Kortshagen, R. U. Carrier Transport in Films of Alkyl-Ligand-Terminated Silicon Nanocrystals. *J. Phys. Chem. C* **2014**, *118*, 19580−19588.

15. Sze, S. M. Physics of Semiconductor Physics, 3rd ed. Wiley-Intersciemce, **2007**, p46

16. Shuai, Z.; Wang, L.; Song, C. Theory of Charge Transport in Carbon Electronic Materials, Springer, **2012**, p13

Schemes and Figures

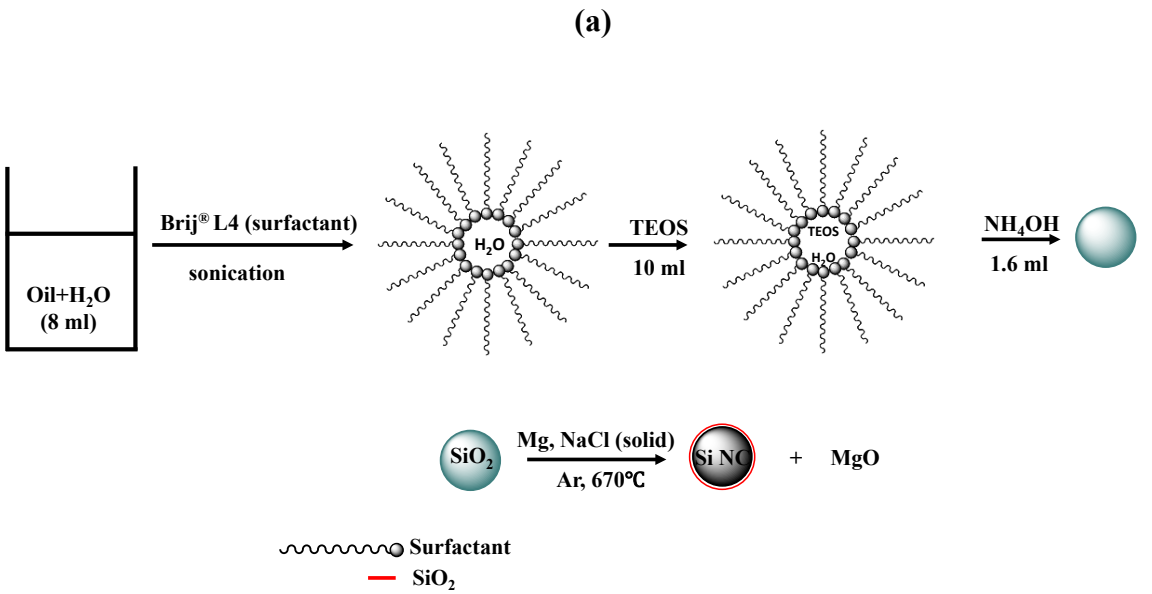

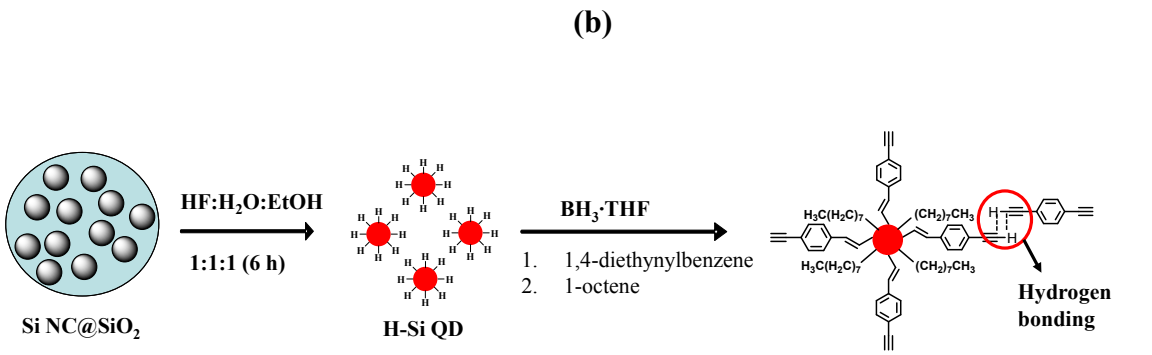

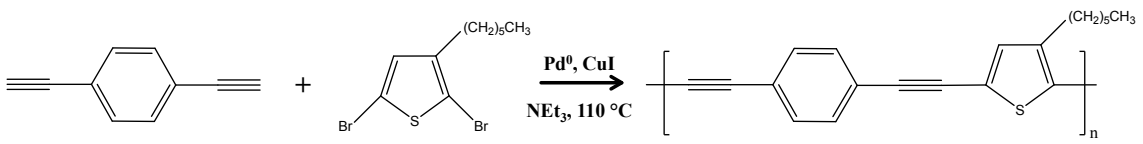

Scheme S1. (a) Synthesis of Si NC@SiO_2. (b) Synthesis of 4-Es/Oct Si QDs. (c) Synthesis of π–conjugated poly(aryleneethynylene) (PAE).

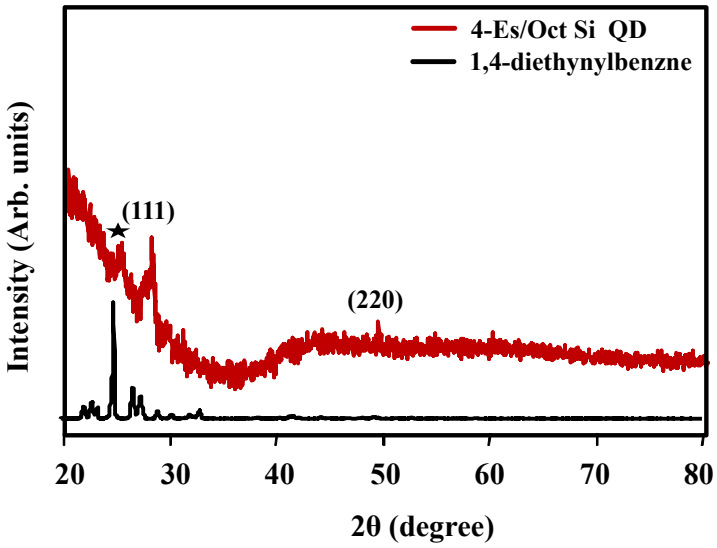

Figure S1. XRD results of 4-Es/Oct Si QD and 1,4-diethynylbenzene.

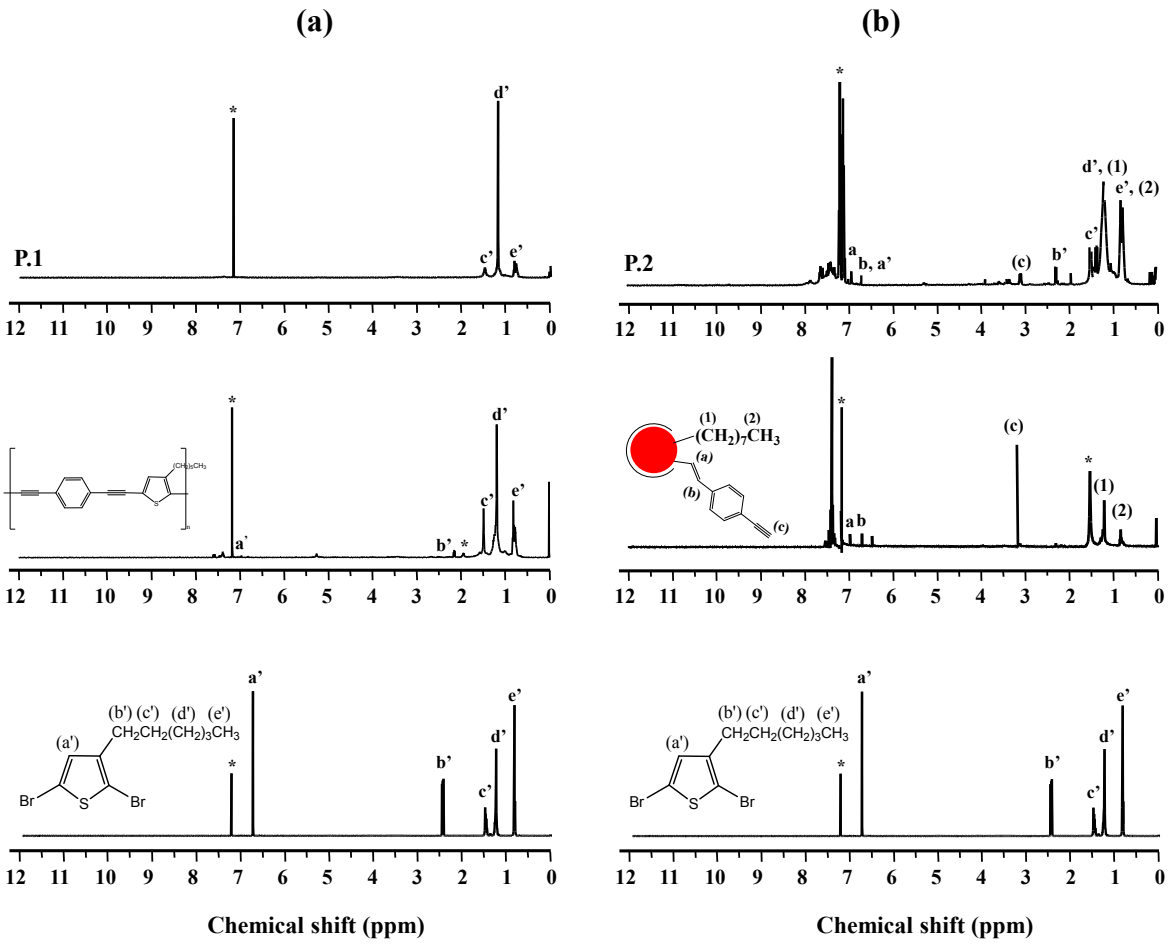

Figure S2. H-NMR spectra of (a) **P.1**, compared with PAE and 2,5-dibromo-3-hexylthiophene, and (b) **P.2**, compared with 4-Es/Oct Si QD and 2,5-dibromo-3-hexylthiophene.

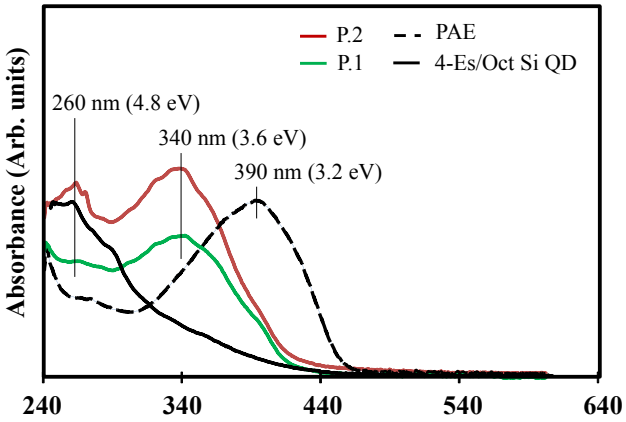

Figure S3. UV–vis absorbance spectra of **P.1** and **P.2** compared with 4-Es/Oct Si QDs and PAE in chloroform.

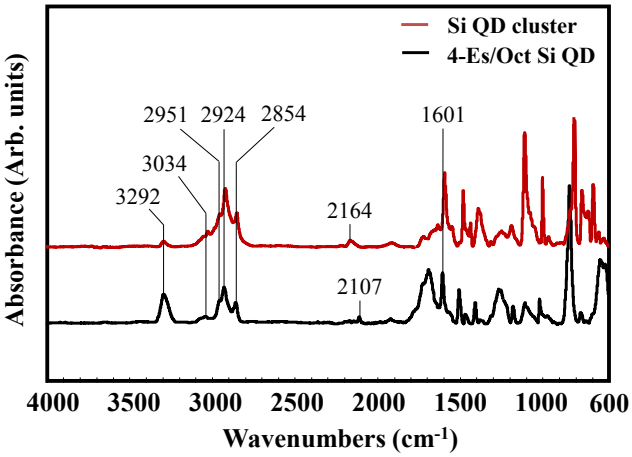

Figure S4. FT-IR spectra of the 4-Es/Oct Si QDs and Si QD clusters.

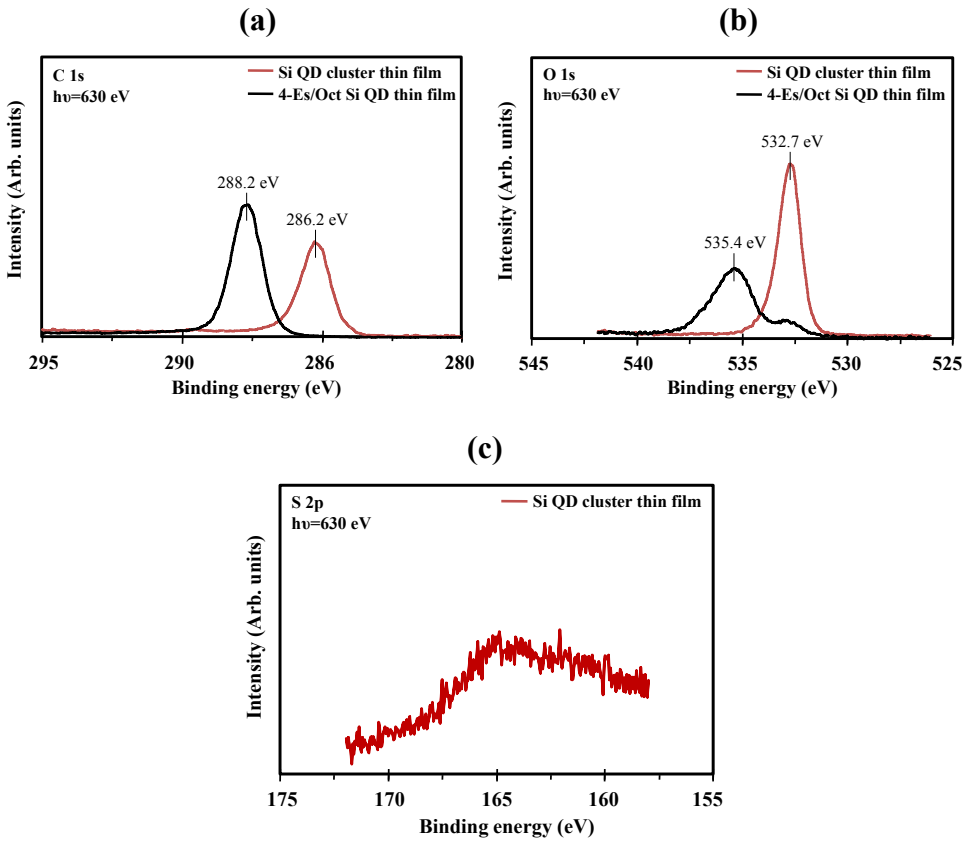

Figure S5. (a) C1s photoemission spectra at photon energy of 630 eV of 4-Es/Oct Si QDs and Si QD cluster thin films curing at 150 °C. Here, the charge-calibration in data analysis is not performed, in order to directly show the different extent of charging for the two thin films. (b) O1s photoemission spectra at photon energy of 630 eV of 4-Es/Oct Si QDs and Si QD cluster thin films cured at 150 °C. Here, the two spectra were charge-calibrated with setting the corresponding C1s peak to 285.0 eV. (c) S1s photoemission spectra at photon energy of 630 eV of Si QD cluster thin film curing at 150 °C. Here, the spectrum was charge-calibrated with setting the corresponding C1s peak to 285.0 eV.